Carbohydrate Polymer Technologies and Applications 5 (2023) 100302

Contents lists available at ScienceDirect

Carbohydrate Polymer Technologies and Applications

journal homepage: www.sciencedirect.com/journal/carbohydrate-polymer-technologies-and-applications

Microstructural influence on physical properties and release profiles of sesame oil encapsulated into sodium alginate-tamarind mucilage hydrogel beads

Stefani Cortés-Camargo [a], Angélica Román-Guerrero [b], Jose Alvarez-Ramirez [c], Erik Alpizar-Reyes [d], Sandra Karina Velázquez-Gutiérrez [e], César Pérez-Alonso [e,*]

[a] Departamento de Nanotecnología, Universidad Tecnológica de Zinacantepec, Av. Libramiento Universidad 106, Col. San Bartolo el Llano, C.P. 51361, Zinacantepec, Estado de México, Mexico
[b] Departamento de Biotecnología, Universidad Autónoma Metropolitana-Iztapalapa, Ferrocarril San Rafael Atlixco No. 186, Col. Leyes de Reforma 1ª. sección, C.P. 09310, México City, Mexico
[c] Departamento de Ingeniería de Procesos e Hidráulica, Universidad Autónoma Metropolitana-Iztapalapa, Ferrocarril San Rafael Atlixco No. 186, Col. Leyes de Reforma 1ª. sección, C.P. 09310, México City, Mexico
[d] Laboratorio de Materiales – LabMAT, Departamento de Ingeniería Civil y Ambiental, Universidad del Bío-Bío, Av. Collao 1202, C.P. 4081112, Concepción, Chile
[e] Departamento de Ingeniería Química, Facultad de Química, Universidad Autónoma del Estado de México, Paseo Colón esq. Paseo Tollocan s/n, Col. Residencial Colón, C.P. 50120, Toluca, Estado de México, Mexico

ARTICLE INFO

Keywords:
Sesame oil
ionic gelation
hydrogel beads
release profiles
structural support
tamarind mucilage

ABSTRACT

Ionic gelation of alginate has become one of the most widely used encapsulation techniques, with the main drawback that alginate hydrogels exhibit highly porous structural networks, which promotes high rates of release of encapsulated core materials. To retard the diffusion and loss of oil, and in turn to develop new alternatives as wall materials, this work aims to analyze the effect of structural properties of hydrogel beads prepared with sodium alginate (SA) and two blends of SA - tamarind seed mucilage (SA-TSM) as wall materials, in the release profiles of sesame oil (SO) encapsulated by ionic gelation. Three emulsions were formed using SA, or SA-TSM blends in mass ratios 1:1 and 1:2, with an SO dispersed phase fraction of 0.02 and mass ratio of wall material:SO 1:1. The resulting emulsions were dropped into a 2.5 % wt. $CaCl_2$ solution to produce three different systems of hydrogel beads. They were characterized by their morphology, size, physical properties, oil encapsulation, swelling, and release performance. According to the results obtained, the hydrogel beads showed an ellipsoidal-like geometry with a mean size of ~2.46 mm. SA-TSM hydrogel beads showed higher encapsulation efficiency (> 73.45%) than SA beads (61.49%). The kinetic curves of SO release showed two regions: a "burst effect" at short times followed by a "lag time" release. The Korsmeyer-Peppas model performed the best fit ($R^2 >$ 0.90) for the release of SO, indicating a diffusion-controlled Fickian transport mechanism for all the beads, the effective diffusion coefficients ranged from 5.18×10^{-11} to 6.46×10^{-11} m^2/s. Therefore, TSM directly influences the structural and physical properties of SA-TSM hydrogel beads, demonstrating efficient structural support and filler function in the formation of wall materials, improving the encapsulation and controlling the release rate of SO in comparison with SA hydrogel beads.

1. Introduction

In recent decades, the use of bioactive compounds, natural additives, and the application of novel techniques for developing healthier products have taken great relevance in the perception of consumers. From the great variety of bioactive compounds used as nutraceuticals, the functionalization with unsaturated fatty acids (UFA) from conventional and non-conventional sources such as chia oil (Us-Medina et al., 2017), walnut oil (Luna-Guevara et al., 2017), sacha inchi oil (da Silva Soares et al., 2019), linseed oil (Menin et al., 2018), fish oil (Di Giorgio, Salgado & Mauri, 2019), and sesame seed oil (SO) (Alpizar-Reyes et al., 2020; Xu-Yan et al., 2012), has been highlighted. Consumption of SO is

* Corresponding author.
E-mail address: cpereza@uaemex.mx (C. Pérez-Alonso).

https://doi.org/10.1016/j.carpta.2023.100302
Received 21 December 2022; Received in revised form 11 February 2023; Accepted 23 February 2023
Available online 25 February 2023

attributed to contributing to strengthening the immune system by enhancing the anti-inflammatory function, improving the lipid profiles in the blood, and displaying further functional properties such as anti-mutagenic activity (Langyan et al., 2022). These properties have been related to the chemical composition of polyunsaturated fatty acids, specifically in SO, the main compounds are linoleic acid (~47%) and oleic acid (~37%), approximately (Langyan et al., 2022; Farhoosh, 2021).

Sesame oil is commonly integrated into food products through different encapsulating systems based on hydrocolloid systems that allow for improving their performance, physicochemical stability, and control release rate, during its processing, storage, and consumption (Velázquez-Gutiérrez et al., 2021; Alpizar-Reyes et al., 2020). Ionic gelation, as an encapsulation technique, is based on the formation of a dispersion or emulsion containing the bioactive compound, and its subsequent injection into the crosslinker solution leading the biopolymer to a gelling process (Alpizar-Reyes et- al., 2022a). This method of encapsulation makes it possible to trap the bioactive compound within the biopolymeric matrix and leave it immobile within a hydrogel bead (Li, Jia & Yin, 2021; Bannikova et al., 2018; Benavides et al., 2016). The advantages in the formation and processing and versatility of the operation mode avoid the use of extreme temperatures that can affect the stability of the core or the wall material. Besides that, pre-treatments are not required, the ionic gelation method is considered a competitive alternative to encapsulate and protect SO, compared to encapsulation techniques such as spray drying, freeze drying, fluidized bed drying, and coacervation.

Among the food-grade hydrocolloids used to build hydrogel beads using ionic gelation stand out proteins and polysaccharides. Sodium alginate (SA) is the most widely used hydrocolloid in the ionic gelation process. This polysaccharide is extracted from brown algae, consisting mainly of covalently linked α-l-guluronic acids (G) and β-d-mannuronic acids (M). It is widely recognized that when SA is in presence of divalent ions, such as Ca^{2+}, the formation of ionic bridges with the chains of this polysaccharide leads to the formation of a gelled system (Yamashita et al., 2021; Zhou et al., 2018). On the other hand, the potential use of beads produced only with SA is focused on the pharmaceutical area (Chen et al., 2018). Specifically, these kinds of beads can be used as models to analyze the lipid digestion process, as is the case with sesame oil, and thus have options to develop drugs that inhibit food digestion, appetite sensations and food intake, increasing satiety and satiation (Ubeyitogullari et al., 2022; Corstens et al., 2017). Another industrial application is the preparation of nutraceutical delivery systems (Li, Wei and Xue, 2021).

The encapsulation of oily compounds using ionic gelation requires pre-treatment for the oil emulsification in the polysaccharide phase, followed by the crosslinking reaction with Ca^{2+} ions and the final drying of the beads (Li, Jia and Yin, 2021; e Silva et al., 2019; Us-Medina et al., 2017). The last step is relevant because it controls the final microstructure of the hydrogel beads (Dehnad, Jafari & Afrasiabi, 2016). Generally, beads obtained with SA produce porous structures that promote immediate delivery of the bioactive compound. For this reason, the use of another biomaterial that acts as a filler agent or structural support allows for hindering and control of the release rates of the encapsulated compound (Velázquez-Gutiérrez et al., 2020; Bušić et al., 2018). For the proper technical development of controlled-release systems, a thorough understanding of the parameters influencing the release rates of encapsulated oils is essential (Boostani & Jafari, 2021; Smaniotto et al., 2021).

The mucilage extracted from the tamarind seed (TSM) has received great attention and interest from the scientific community in recent years, especially due to its physicochemical, thermal, rheological, and functional properties, making it suitable for being used as an emulsifying agent and wall material in the process of encapsulation of bioactive lipophilic compounds (Alpizar-Reyes et al., 2022b). TSM is amphiphilic, with a molecular weight ranging between 700-880 kDa, mainly constituted of polysaccharides such as glucose, galactose, and xylose, with 14.24% of protein content (Alpizar-Reyes et al., 2018, Alpizar-Reyes et al., 2017a).

Therefore, this work describes for the first time, the use of blends of SA and TSM for the encapsulation of SO through ionic gelation process, opening a new window for the use of TSM as filler material in the egg-box structure of alginate hydrogels. The hypothesis to be tested in this work is that the addition of the TSM in the conformation of the wall material directly influences the structural and physical properties of the hydrogel beads and affects the release profiles of the SO encapsulated in comparison with beads formulated only with SA. In this regard, the present study focuses on the analysis of the main factors that impact the release of SO from hydrogel beads made from blends of TSM-SA, acting as wall materials, and evaluating the particle properties and release profiles for the SO.

2. Materials and methods

2.1. Materials

Sodium alginate (SA; Protanal® RF 6650 Alginate; 65% guluronic acid with a purity of 90%) was gently provided by FMC Health & Nutrition (Mexico City, Mexico). Tamarind dried pods and sesame seeds were acquired at a supermarket in the city of Toluca (State of Mexico, Mexico). TSM was extracted and obtained as a powder following the procedure used by Alpizar-Reyes et al. (2017b). Sesame seed oil (SO) was extracted according to Velázquez-Gutiérrez et al. (2020). A cold press extraction of sesame seeds was used with a maximum pressure of 8.8×10^8 N/m^2 applied by the piston at 20 ± 2°C. The extracted SO was placed in amber bottles and stored at 4°C until use. All experimental runs were made by employing deionized water. Chemical reagents were of analytical grade (Sigma Aldrich, Toluca City, Mexico).

2.2. Emulsion formulation and preparation of hydrogel beads

Three dispersions of the different wall materials were prepared with deionized water, SA (2% w/v), and two blends of SA-TSM (2% w/v) in weight ratios of 1:1 and 1:2, respectively. The solutions were overnight shaken at room temperature (~20°C) for a complete biopolymer's hydration. Biopolymer dispersions were degassed for 12 h before use. The conditions for the formation of O/W emulsions were defined in preliminary assays, then a mass dispersed phase fraction of 0.02 (2g SO/100g emulsion), was slowly added into each biopolymer dispersion, using a core:wall material mass ratio of 1:1. The homogenization was performed with an Ultra-Turrax T50 homogenizer (IKA®-WERKE Works Inc., Wilmington, NC, USA) at 6400 rpm during 5 min (Benavides et al., 2016).

For the hydrogel beads production, 10 mL of each emulsion was taken with a syringe (0.70 mm tip diameter of the needle). Subsequently, the tip of the needle was placed at 30 cm above the beaker containing 100 mL of calcium chloride solution ($CaCl_2$, 2.5% w/v) with continuous mechanical stirring at 250 rpm, and the emulsion was dropped at a rate of 20 drops per minute. The beads were left to stand in the stirred $CaCl_2$ solution for 40 min at room temperature to let them harden. Finally, the beads were rinsed with deionized water, filtered (mesh size of 355 μm), dried at 50°C in an oven for 24 h, and stored in amber bottles until use (Velázquez-Gutiérrez et al., 2020). Hydrogel beads formed with solely SA were considered blank (SA), and the beads containing SA-TSM ratios of 1:1 and 1:2 were identified as B1 and B2, respectively.

2.3. Physical properties of hydrogel beads

2.3.1. Hydrogel bead morphology and sphericity factor (SF)

The surface appearance and bead morphology were examined using a scanning electron microscope (SEM) model JSM-IT100 (Jeol Co. Ltd.,

Tokyo, Japan). Samples were coated with gold for 5 s and mounted on SEM stubs with double-sided adhesive tape (Ted Pella, Redding, California, USA). Images were taken at an accelerating voltage of 8 kV with a magnification of 30 × .

The sphericity factor (*SF*) is a shape distortion parameter; when this value is smaller than 0.5, it is assumed that beads are spherical. Equation (1) was used to calculate *SF* (Chan, 2011):

$$SF = \frac{D_{\max} - D_{per}}{D_{\max} + D_{per}} \tag{1}$$

Here, D_{max} = Maximum diameter of the bead (mm), D_{per} = Perpendicular diameter to $D_{\max}$ (mm).

2.3.2. Moisture content

The moisture content of hydrogel beads was obtained by using the gravimetric method. Hydrogel beads were oven-dried at 105°C until achieving constant weight.

2.3.3. Bulk and tapped density

Bulk density (ρ_b) was estimated by weighing 10 g of hydrogel beads sample (m_0) and transferred into a 10 mL glass graduated cylinder. The occupied volume was registered directly (v_b). For tapped density (ρ_t), the graduated cylinder containing the sample was tapped manually until a constant volume reading (v_t). Calculations for both densities were as follows:

$$\rho_b = \frac{m_0}{v_b} \tag{2}$$

$$\rho_t = \frac{m_0}{v_t} \tag{3}$$

2.3.4. Flowability

Flowability is the capacity to flow freely and regularly without obstruction, this property was determined based on the compressibility index (*CI*) and the Hausner ratio (*HR*) as follows:

$$CI = \frac{\rho_t - \rho_b}{\rho_t} \tag{4}$$

$$HR = \frac{\rho_t}{\rho_b} \tag{5}$$

where ρ_b and ρ_t are the bulk and tapped densities, respectively.

2.3.5. Particle density and particle porosity

The particle density ($\rho_{particle}$) of hydrogel beads was measured based on the method by Chew, Tan & Nyam (2018). Briefly, 5 mL of petroleum ether was added to a 10 mL glass graduated cylinder that contained one gram of hydrogel beads sample (m_p), and the cylinder was shaken to suspend the beads. Finally, 1 mL of the same solvent was added to rinse down possible hydrogel particles stuck on the container's wall. Total volume occupied (v_p) was registered, and Equation (6) was utilized to calculate the particle density.

$$\rho_{particle} = \frac{m_b}{v_p - 6} \tag{6}$$

Particle porosity was estimated using the ratio between particle and tapped densities of hydrogel beads: $\varepsilon = 1 - \rho_t/\rho_{\text{particle}}$

$$\varepsilon = 1 - \left(\frac{\rho_t}{\rho_{particle}}\right) \tag{7}$$

2.4. Ionic gelation process yield (Y%)

Process yield is a measure of the rate between the number of hydrogel beads obtained (M_b) and the emulsion dispersion (M_{em}) spent for their formation, it was calculated using Equation (8):

$$Y(\%) = \frac{M_b}{M_{em}} \times 100 \tag{8}$$

2.5. SO encapsulation efficiency (EE%) and loading capacity (LC%)

The encapsulation efficiency (EE%) was determined using the method reported by Velázquez-Gutiérrez et al. (2020). Briefly, the surface oil ($O_{surface}$) was determined after extracting the SO with n-hexane from the hydrogel beads for 60 s. The total oil (O_{total}) amount was determined gravimetrically after 6 h of Soxhlet extraction with n-hexane from the hydrogel beads sample (W_{beads}). EE (%) and LC (%) were evaluated as follows:

$$EE(\%) = \frac{\left(O_{total} - O_{surface}\right)}{O_{total}} \times 100 \tag{9}$$

$$LC(\%) = \frac{O_{total}}{W_{beads}} \times 100 \tag{10}$$

This method makes it possible to determine the amount of oil present within the hydrogel beads, eliminating other compounds that may interfere and reducing the steps for sample processing by considering the oil phase as a material with a defined composition.

2.6. Swelling index (SI)

The swelling index *(SI)* of hydrogel beads was obtained at different time intervals within 4 h. For this, 0.5g of the sample were poured into 15 mL of deionized water and maintained in contact for the appropriate time at room temperature. After draining the extra water using filter paper, the enlarged beads were weighed, and Equation (11) was used to calculate *SI*:

$$SI(\%) = \frac{W_t - W_0}{W_0} \times 100 \tag{11}$$

where W_t and W_0 represent the weight of the hydrogel beads at time t and the beginning of the experiment, respectively.

2.7. Sesame oil release from hydrogel beads

Release kinetics were evaluated at 25°C, 12 beakers of 50 mL containing one gram of hydrogel beads (previously washed with n-hexane for 60 s to remove surface oil) and 20 mL of *n*-hexane were slowly mechanical stirred, the beads were removed by filtration from the beakers at different time intervals (from 0 to 180 min). Afterward, the supernatants and the beads were kept overnight in an oven at 35°C to evaporate the solvent. Finally, the released oil from hydrogel beads was measured by taking the difference between the weight of the oil removed with solvent after drying and the weight of the beads used (Goyal et al., 2016).

2.7.1. Kinetics of release

Data obtained for the release of SO from hydrogel beads was fitted to distinct kinetic and release models (zero and first order, Higuchi, Hixson-Crowell and Korsmeyer-Peppas) to reveal the transport mechanism (Dangi et al., 2022). The following equations were used for determining the diffusion coefficients (Beirão da Costa et al., 2012):

$$\frac{M_t}{M_\infty} = 6\left(\frac{Dt}{\pi r^2}\right)^{0.5} - \left(\frac{3Dt}{r^2}\right) \qquad for \qquad \frac{M_t}{M_\infty} \geq 0.7 \tag{12}$$

$$\frac{M_t}{M_\infty} = 1 - 0.61\exp\left(-\frac{Dt\pi^2}{r^2}\right) \qquad for \qquad \frac{M_t}{M_\infty} \geq 0.7 \tag{13}$$

where M_t and M_∞ are the mass of SO released at time t and the amount of SO removed when equilibrium was reached respectively, D is the

diffusion coefficient, and *r* is the radius of the hydrogel bead.

2.8. Statistical analysis

All the treatments were done in triplicate and reported as mean values and standard deviation. One-way ANOVA and Tukey's test at a significant level of $p<0.05$ was used for establishing significant differences. The statistical analysis was done using Minitab version 16.0 software (Minitab Inc., State College, PA, USA).

3. Results and discussion

3.1. Physical properties of hydrogel beads

3.1.1. Hydrogel bead morphology, size and sphericity factor (SF)

The SEM images for the hydrogel beads systems are shown in Fig. 1, which exhibited an ellipsoidal-like geometry. The SA beads (Fig. 1a) show a less smooth external surface compared to SA-TSM beads (Fig. 1 b and c) which do not show apparent cracking, indicative of the function of TSM as filler, producing important changes in the microstructure of the hydrogel beads. Cross-section cuts images (Fig. 1 d, e and f) also show differences in the beads with and without TSM. SA beads exhibit a more porous structure, while SA-TSM in B1 and B2 displayed a more homogeneous internal structure with a reduction of internal cracks, suggesting the presence of structural support functionality due to the presence of the mucilage. Lozano-Vazquez et al. (2015) produced hydrogel beads using different ratios of SA and modified tapioca starch, their findings reveal the function of starch molecules as a filler agent on the surface of the SA hydrogel. The SEM results revealed that beads produced only with SA showed fissures in their surface and probably inner holes, while the beads made with SA-starch exposed a highly tortuous porous structure, suggesting a structural support action promoted by starch, similar to that behavior observed in the samples made with SA-TSM function evaluated in this study.

The mean particle size of the hydrogel beads ranged from 2.09 to 2.91 mm for all the systems studied, increasing in magnitude as the TSM content was increased (see Table 1). This behavior can be associated with an increase in the viscosity of the emulsion caused by the addition of TSM, producing the formation of larger drops during the dripping step while the gelation process occurs leading to larger beads. Previous reports, where hydrogel beads based on SA-polysaccharide blends, have reported particle sizes ranging between 2.06-2.19 mm for SO encapsulated in SA-nopal mucilage (Velázquez-Gutiérrez et al., 2020); 1.74-2.16 mm dor chia oil encapsulated in SA-chia mucilage produced with a peristaltic pumping with a Masterflex hose (2 mm inner diameter) to an eight-nozzle dispensing disc, and dropped into a $CaCl_2$ solution at different times of harden (Us-Medina et al., 2017).

According to the sphericity factor (*SF*; Table 1), the beads did not exhibit a spherical shape ($SF > 0.05$). The beads containing TSM had lower *SF* than that for SA beads, which could be attributed to the occurrence of stronger cross-linking interactions that led to a more compact and homogeneous structure due to structural support given by the TSM to SA beads (Fig. 1) (Zhou et al., 2018; Lozano-Vazquez et al., 2015). Lower *SF* values, close to 0.05, have been reported for SO encapsulated in SA-nopal mucilage beads and in SA-modified tapioca

Table 1
Physical properties of hydrogel beads.

	SA	B1	B2
Size (mm)	2.09 ± 0.11^{c}	2.39 ± 0.10^{b}	$2.91\pm 0.05a^{a}$
Sphericity Factor	0.17 ± 0.00^{a}	0.09 ± 0.00^{c}	0.12 ± 0.00^{b}
Moisture Content (%)	2.96 ± 0.23^{b}	3.47 ± 0.32^{b}	4.41 ± 0.14^{a}
Bulk Density (g/cm^3)	0.42 ± 0.01^{c}	0.56 ± 0.01^{b}	0.69 ± 0.01^{a}
Tapped Density (g/cm^3)	0.45 ± 0.00^{c}	0.61 ± 0.01^{b}	0.71 ± 0.01^{a}
Carr's Index	0.07 ± 0.01^{a}	0.08 ± 0.00^{a}	0.03 ± 0.01^{b}
Hausner Ratio	1.07 ± 0.01^{b}	1.09 ± 0.00^{a}	1.03 ± 0.01^{c}
Particle Density (g/cm^3)	1.41 ± 0.01^{c}	1.25 ± 0.01^{a}	1.02 ± 0.01^{b}
Particle Porosity	0.68 ± 0.02^{a}	0.51 ± 0.02^{b}	0.30 ± 0.01^{c}

SA: Sodium alginate; B1 and B2: Sodium alginate - Tamarind seed mucilage (1:1 and 1:2), respectively.
Values are means ± standard deviation of three replicates. Superscripts with different letters in same row indicate significant differences ($p \leq 0.05$).

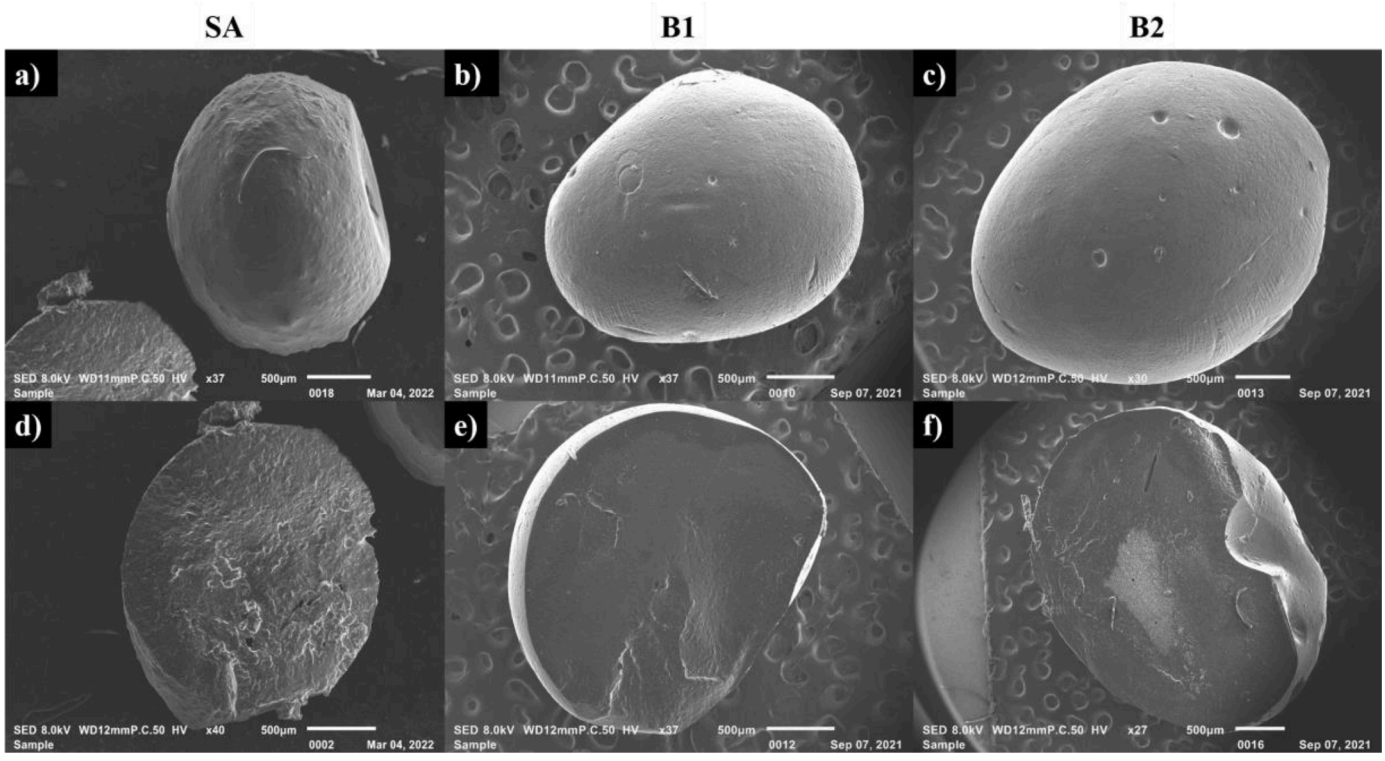

Fig. 1. SEM images of external and cross-sectional aspect of the different hydrogel beads. (a) and (b) SA; (b) and (e) B1; (c) and (f) B2.

starch beads, indicating that the morphology of SA beads is influenced by the type of wall material and the production method (Velázquez--Gutiérrez et al., 2020; Lozano-Vazquez et al., 2015).

3.1.2. Moisture content

Moisture content is an essential parameter since it plays a critical role in the physical and chemical stability and textural properties of foods. Table 1 showed that SA-TSM hydrogel beads had higher moisture contents than beads made only with SA, associated with the greater water-holding capacity of TSM. These percentages of moisture content for the three systems produced are below the minimum allowable moisture value (6%) to avoid the risk that the hydrogel beads may suffer bacterial contamination (Bajac et al., 2022).

3.1.3. Bulk and tapped density

Bulk densities ranged from 0.42 to 0.69 g/cm^3, being B2>B1>SA beads. The higher content of TSM in the beads led to higher bulk densities, denoting a more compacted structure and a lower amount of air entrapped within the particles, contributing to the stabilization of the oil encapsulated by decreasing the oxygen availability and therefore minimizing the oil degradation. Thus, bulk density in the SA and SA-TSM hydrogels is influenced by the morphology, particle size, and final structure of the gelled polysaccharides (Chew, Tan & Nyam, 2018; Premi & Sharma, 2017). Tapped density is a significant parameter for packaging, transportation, and commercialization of solid products, the greater the tapped density, the fewer containers for storage and easier handling are required. (Chew, Tan & Nyam, 2018; Premi and Sharma, 2017). In this sense, B2 hydrogel beads displayed higher tapped density followed by B1, and SA.

3.1.4. Flowability

CI and *HR* are two parameters commonly used to describe the flowing properties of particles during food processing operations. *CI* indicates the agglomeration capacity of particles (cohesivity); meanwhile, *HR* determines the friction force. When *HR* and *CI* become greater, the flowability decreases. According to the results shown in Table 1, the hydrogel beads made with SA and SA-TSM had "excellent flowability", since their $CI < 10$ and their $HR < 1.11$ (Bajac et al., 2022; Dima et al., 2016; Bakry et al., 2016). B2 hydrogel beads showed the lowest values of *CI* and *HR*, which could be related to their larger size and lower surface oil content, which helped to reduce the beads' stickiness and enhance their flowability (Premi and Sharma, 2017).

3.1.5. Particle density and particle porosity

Particle density considers the total volume and particle weight, excluding the void spaces in the material (López-Ortiz et al., 2016; Fernandes et al., 2013). According to the results shown in Table 1, the hydrogel beads formed only with SA had a higher particle density and smaller particle size that promote a denser packing and higher compression between the beads (Premi and Sharma, 2017). On the other hand, particle porosity is usually described as a measure of the sample void fraction, herein B2 beads displayed lower porosity with robust structure. These features can be attributed to the major content of TSM on the hydrogel bead matrix that acted as filler, reducing the volume of voids in the beads. Based on previous reports, prolonged storage stability in the encapsulation systems is achieved when the particles display high bulk density and low particle porosity, providing better manageability (Chew, Tan & Nyam, 2018; Premi and Sharma, 2017).

3.2. Ionic gelation process yield (Y%)

The yield percentages for the hydrogel beads were higher than 70% (Table 2), suggesting that the encapsulation process of the SO by ionic gelation had a minor loss. The process yield in B2 beads was significantly higher than that obtained for B1 beads and SA beads. These results are correlated to the higher content of TSM in B2 that generates more robust and stronger cross-linked networks between SA, TSM and calcium ions (Velázquez-Gutiérrez et al., 2020; Bera et al., 2015). Similar results were obtained for SO encapsulated in hydrogel beads formed with SA and blends of SA-nopal mucilage (72.5 - 91.7 %), where the larger amount of mucilage integrated into the wall material led to higher efficiencies in the encapsulation process (Velázquez-Gutiérrez et al., 2020).

Table 2
Process yield, Surface oil, *EE* and *LC* of hydrogel beads.

	SA	B1	B2
Yield (%)	70.50 ± 0.42^{c}	75.94 ± 1.12^{b}	89.08 ± 1.44^{a}
Surface Oil (%)	7.78 ± 0.16^{a}	6.65 ± 0.13^{b}	5.11 ± 0.24^{c}
EE (%)	61.49 ± 0.37^{c}	73.45 ± 0.35^{b}	84.63 ± 2.03^{a}
LC (%)	20.20 ± 0.29^{c}	25.05 ± 0.11^{b}	33.24 ± 0.32^{a}

SA: Sodium alginate; B1 and B2: Sodium alginate - Tamarind seed mucilage (1:1 and 1:2), respectively.
Values are means ± standard error, of three replicates. Superscripts with different letters in same row indicate significant differences ($p \leq 0.05$).

3.3. Encapsulation efficiency (EE%) and loading capacity (LC%)

Table 2 shows the surface oil content, encapsulation efficiency (EE %), and loading capacity (*LC*%) for the three hydrogel beads systems. SA beads displayed a significantly higher amount of surface oil followed by B1 and B2 beads, these results suggest that the larger porosity observed in the SA hydrogel beads facilitates the diffusion of SO from the hydrogel matrix to their surface, reducing their capacity to contain the SO entrapped in the core of the encapsulating system (Velázquez-Gutiérrez et al., 2020).

Regarding *EE*, a similar trend was observed, B2 achieved the highest *EE* followed by B1 and SA, respectively. These results restate the fact that chemical the composition of the polysaccharides used as wall materials influenced the performance of their functional properties, in the case of TSM, this polysaccharide has a significant protein content (12.77 - 15.40 %) that contributes to its great capacity to retain oily phases and improve their stability in the emulsions used to produce the hydrogel beads (Zeeb et al., 2015; Carneiro et al., 2013). On the other hand, *LC* measures the amount of SO that a bead can hold and depends on the amount of the biopolymer used. Higher values mean that lower quantities of beads are required for accomplishing the desired functional properties in the final applications. As can be seen in Table 2, SA beads had the lowest *LC* value, suggesting the formation of a less robust and highly porous microstructure that promotes and facilitates the release of the oil phase, contrary to that observed in B2 where a better oil phase inclusion was achieved (33.24 ± 0.32%) (Velázquez-Gutiérrez et al., 2020; Menin et al., 2018; Benavides et al., 2016).

3.4. Swelling index (SI)

To analyze how the swelling process happens on TSM hydrogel beads, the profile of *SI* against time was plotted in Fig. 2 during the first four hours after their formation. Hydrogel beads made with SA-TSM exhibited a greater swelling index under all the examined timeframes than SA beads. According to Fig. 2, the hydrogel beads swelled for up to 60 min, followed by a decrease in the swelling rate (deswelling). This swelling/deswelling behavior can be ascribed to the fact that the solid bead is made up of cross-linked polymer chains that tend to swell when in contact with the aqueous solution, causing relaxation and expansion of the polymer. Once maximum swelling is reached by the bead, the polymer in the solution tends to erode leading to deswelling (Kassem et al., 2015; Sudipto et al., 2002).

The formulation B2 showed the highest water absorption rate and moisture sensitivity, and higher swelling properties than those observed for the SA hydrogel beads. Ban et al. (2022) stated that the use of filler agents in cross-linked hydrocolloids can increase the swelling degree of

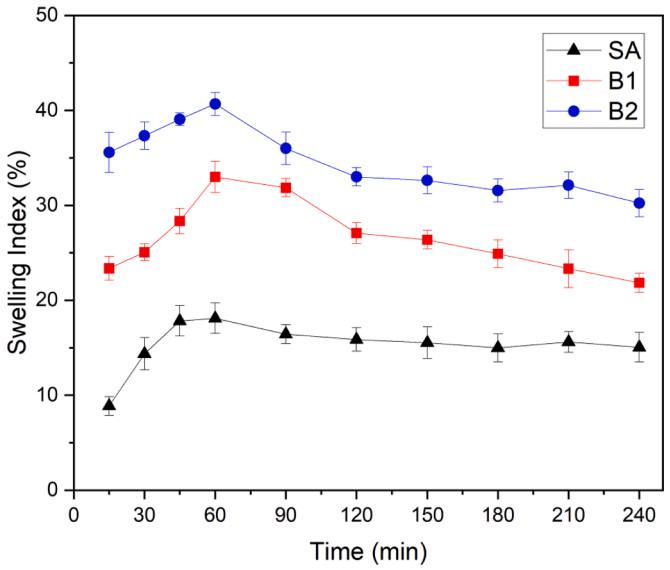

Fig. 2. Swelling index profiles of hydrogel beads at 25°C.

the hydrogel systems. In this case, the use of TSM as a filler agent for the SA hydrogels contributed to increasing the hydrophilic capability of the beads, where the high swelling ratio of the SA-TSM hydrogel beads is indicative of a porous structure with highly connected caverns that allows the easy adsorption of water (Lozano-Vazquez et al., 2015; Alpizar-Reyes et al. 2017a).

3.5. SO released from hydrogel beads

Fig. 3 presents the kinetic curves of SO release from hydrogel beads at room temperature, the three bead systems displayed two regions. The first region was observed during the first 30 min of contact between the beads and the liquid medium, all the systems showed a "burst effect" where a considerable percentage of SO is released in a relatively short period. This might be due to the number of oil molecules on the surface of the beads that were not enough linked into the structure and so, were easily released from particles to the bulk phase. From Fig. 3, it can be observed that SA hydrogel beads showed higher SO release percentages, attributed to their inferior oil retention capacity. For SA-TSM beads, the lower SO release may be related to the protein content present in TSM,

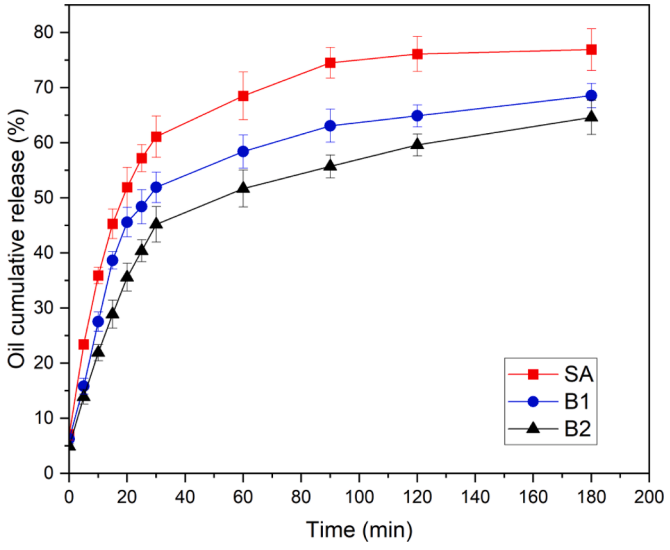

Fig. 3. Cumulative release profiles of hydrogel beads at 25°C.

which acts as an emulsifier enhancing the stability of the emulsions and providing better retention of SO within the biopolymer matrix. Despite the SA-TSM hydrogels beads offering a higher percentage of swelling than SA beads in the burst region (see Fig. 2), the release rate of SO from the beads was slower in SA-TSM than that in SA beads (Fig. 3), inferring that the matrices formed by the combination of both SA and TSM polymers led to a more robust and less porous structure, with higher tortuosity, confirming the role played by the TSM as structural support for the SA-based hydrogels.

From Fig. 3, the second region shows quasi-constant release profiles after 60 min, indicating a sustained release referred to as "lag time". This region is characterized by linear oil concentration gradients in the beads over relatively large time intervals, exhibiting a slow-release rate associated with the development of diffusive processes, in which the effective diffusivity remains practically constant and exhibits the lowest values. According to Fig. 3, the SA-TSM beads displayed a lower percentage of SO release than SA beads, agreeing with the hypothesis that TSM modifies the structure of the SA hydrogel by acting as filler and reducing its porosity, increasing the tortuosity in the polysaccharide matrix, delaying the transport of the oil from the core to the surface by allowing the water adsorption on the surface of the beads and contributing to block the beads pores hindering the oil diffusion (Beirão-da-Costa et al., 2013; Beirão-da-Costa et al., 2012; Bera et al., 2015; López Córdoba et al., 2013). Besides the effect of the larger particle size of the beads to the reduction on the surface area that modulates the release profile of the core material (Boostani & Jafari, 2021; Maderuelo et al., 2011).

Regarding the kinetic modeling, data for the SO release were fitted to zero-order, first-order, Higuchi, Hixon-Crowell, and Korsmeyer-Peppas models, the results are given in Table 3. The best fitting model was Korsmeyer-Peppas for all the hydrogel beads systems ($0.9042 < R^2 < 0.9447$). This model permits to descript and classify of the diffusion mechanisms associated with the release of SO from the hydrogel beads, specifically through the magnitude of the parameter "n". Based on its magnitude, the release mechanism classification is defined as Case I. Fickian diffusion if $n \leq 0.43$; anomalous or non-Fickian transport when $0.43 < n < 0.85$; Case II. Zero-order release if $n = 0.85$ (Dyab et al., 2018; Siepmann & Peppas, 2001); and "Supra II" type transport for $n > 0.89$ (Dash et al., 2010). Based on the results of this work, the Fickian transport mechanism governs the mass transfer in the SA and SA-TSM beads, where the SO release is controlled by the oil diffusion through the geloid matrix. Furthermore, when TSM content was increased in the beads systems, the release rate constant (k) values decreased significantly ($p<0.05$) indicating a reduction in the release rate (Wu et al., 2014).

Regarding the effective diffusion coefficients for SA and SA-TSM beads, their values were calculated at each oil release region and the values are reported in Table 4. For the first region ($t \leq 30$ min), as the TSM content increased in the SA-TSM bead, the effective diffusion coefficient was higher, which from a mass transfer point of view, the release rate of SO might be higher for B1 and B2 hydrogel beads, however, the role of TSM as structural support generated more compact and robust structures that diminished the percentage of SO released (Fig. 3). For the second region of oil release, the effective diffusion coefficients remained practically constant ($\sim 6 \times 10^{-11}$ m^2/s), evidencing a sustained release profile between 30 to 180 min time interval for all the SA and SA-TSM beads systems.

4. Conclusions

The results obtained in this study bring useful information about the use of TSM as a filler agent for improving the functional properties of SA-based hydrogel beads as carriers and protecting agents for SO. TSM showed to be effective as a structural support that promotes the formation of more robust and complex networks when producing hydrogel beads by ionic gelation. The encapsulation and release properties of SO

Table 3
Kinetic parameters for the release of SO from the hydrogel beads systems.

Model	SA	B1	B2
Zero order $Q = kt + Q_0$	$Q = 0.0003t + 0.0370$	$Q = 0.0003t + 0.0302$	$Q = 0.0003t + 0.0240$
$k \times 10^5$ **(min^{-1})**	30.0 ± 9.0[a]	30.0 ± 7.0[a]	30.0 ± 10.0[a]
Q_0 **(g)**	0.0370 ± 0.016[a]	0.0302 ± 0.011[a]	0.0240 ± 0.006[a]
R^2	0.5940	0.5768	0.7154
First order $Q = Q_0 exp(kt)$	$Q = 0.0411\exp(0.0044t)$	$Q = 0.0341\exp(0.0047t)$	$Q = 0.0282\exp(0.0054t)$
$k \times 10^5$ **(min^{-1})**	440.0 ± 50.0[a]	470.0 ± 30.0[a]	540.0 ± 9.0[b]
Q_0 **(g)**	0.0411 ± 0.010[a]	0.0341 ± 0.009[a]	0.0282 ± 0.009[b]
R^2	0.5076	0.4782	0.6132
Higuchi $Q = kt^{1/2}$	$Q = 0.0077t^{1/2}$	$Q = 0.0066t^{1/2}$	$Q = 0.0059t^{1/2}$
$k \times 10^5$ **(min$^{-1/2}$)**	770.0 ± 3.0[a]	660 ± 7.0[b]	590.0 ± 9.0[c]
R^2	0.5571	0.6422	0.8097
Hixson-Crowell $Q^{1/3} = kt + Q_0^{1/3}$	$Q^{1/3} = 0.0006t + 0.0342$	$Q^{1/3} = 0.0006t + 0.0330$	$Q^{1/3} = 0.0007t + 0.3001$
$k \times 10^5$ **(min^{-1})**	60.0 ± 9.0[a]	60.0 ± 9.0[a]	70.0 ± 1.0[b]
Q_0 **(g)**	0.0342 ± 0.007[a]	0.0330 ± 0.008[a]	0.3001 ± 0.020[b]
R^2	0.5339	0.5082	0.6448
Korsmeyer-Peppas $Q = kt^n$	$Q = 0.0231t^{0.2508}$	$Q = 0.0178t^{0.2749}$	$Q = 0.0127t^{0.3253}$
$k \times 10^5$ **(min^{-n})**	2310.9 ± 900[a]	1780.0 ± 200[b]	1270.0 ± 800[c]
n	0.2508 ± 0.020[a]	0.2749 ± 0.005[b]	0.3253 ± 0.009[c]
R^2	0.9278	0.9042	0.9447

SA: Sodium alginate; B1 and B2: Sodium alginate - Tamarind seed mucilage (1:1 and 1:2), respectively.
Q: Sesame oil quantity released at time t; Q_0: Initial sesame oil quantity released; k: Release rate constant; n: Diffusional exponent; R^2: Correlation coefficient.
Values as means ± standard error for three replicates are provided. Different letters in the same row indicate statistically significant differences ($p \leq 0.05$).

Table 4
Diffusion coefficients for the different bead formulations.

Diffusion Coefficients (m^2/s)	SA	B1	B2
$\frac{M_t}{M_\infty} \leq 0.7$	5.18×10^{-11}	5.59×10^{-11}	6.45×10^{-11}
R^2	0.9373	0.8775	0.9209
$\frac{M_t}{M_\infty} > 0.7$	6.23×10^{-11}	6.46×10^{-11}	6.39×10^{-11}
R^2	0.9806	0.9478	0.9560

SA: Sodium alginate; B1 and B2: Sodium alginate - Tamarind seed mucilage (1:1 and 1:2), respectively.
M_t: Sesame oil mass released at time t; M_∞: Sesame oil mass released at equilibrium; R^2: Correlation coefficient.
Data are presented as means ± SD (n=3).

resulted enhanced when TSM was added to the hydrogel formulations, opening new alternatives in the selection, design, and use of non-conventional wall materials suitable to satisfy a great variety of industrial applications. Despite the TSM content on the SA-TSM beads, all the systems exhibited ellipsoidal-like geometry, a more homogeneous structure with a less cracking and smoother surface, but larger particle size. Retardation on the SO transport and release from the core to the surface of the beads was modulated by the TSM content in the SA-based hydrogels, better encapsulation efficiencies and retarded released profiles could be associated with the high protein content associated with the TSM molecule. The release profiles of SO from the SA-based hydrogels displayed two main regions, the first one with a "burst effect" where a substantial percentage of SO was rapidly released, and a quasi-constant release profile related to a sustained SO release. According to the results, the encapsulation of SO in SA-TSM blends as wall materials in encapsulation systems formed by ionic gelation had better structural and physical properties compared to those formed only with SA.

CRediT authorship contribution statement

Stefani Cortés-Camargo: Conceptualization, Methodology, Formal analysis, Investigation, Writing – original draft. **Angélica Román-Guerrero:** Validation, Writing – review & editing. **Jose Alvarez-Ramirez:** Formal analysis, Writing – review & editing, Supervision. **Erik Alpizar-Reyes:** Methodology, Formal analysis, Data curation, Writing – original draft. **Sandra Karina Velázquez-Gutiérrez:** Methodology, Software, Validation. **César Pérez-Alonso:** Validation, Resources, Writing – review & editing, Supervision.

Declaration of Competing Interest

The authors declare that they have no known competing financial interests or personal relationships that could have appeared to influence the work reported in this paper.

Data availability

Data will be made available on request.

Acknowledgements

The authors wish to acknowledge the partial financial support of this research to the Universidad Autónoma del Estado de México through grant 6661/2022SF.

References

Alpizar-Reyes, E., Román-Guerrero, A., Cortés-Camargo, S., Velázquez-Gutiérrez, S. K., & Pérez-Alonso, C. (2022a). Recent approaches in alginate-based carriers for delivery of therapeutics and biomedicine. In S. Jana, S. Jana, & A. Domb (Eds.), *Polysaccharide-based Biomaterials* (pp. 27–68). London, UK: The Royal Society of Chemistry. ISBN 978-1-83916-498-9.

Alpizar-Reyes, E., Cortés-Camargo, S., Román-Guerrero, A., & Pérez-Alonso, C. (2022b). Tamarind gum as a wall material in the microencapsulation of drugs and natural products. In S. Jana, & S. Jana (Eds.), *Micro- and nanoengineered gum-based biomaterials for drug delivery and biomedical applications* (pp. 347–382). Amsterdam, Netherlands: Elsevier. ISBN 978-0-323-90986-0.

Alpizar-Reyes, E., Carrillo-Navas, H., Gallardo-Rivera, R., Varela-Guerrero, V., Alvarez-Ramírez, J., & Pérez-Alonso, C. (2017a). Functional properties and physicochemical characteristics of tamarind (*Tamarindus indica* L.) seed mucilage powder as a novel hydrocolloid. *Journal of Food Engineering, 209*, 68–75. https://doi.org/10.1016/j.jfoodeng.2017.04.021

Alpizar-Reyes, E., Carrillo-Navas, H., Romero-Romero, R., Varela-Guerrero, V., Alvarez-Ramírez, J., & Pérez-Alonso, C. (2017b). Thermodynamic sorption properties and glass transition temperature of tamarind seed mucilage (*Tamarindus indica* L.). *Food and Bioproducts Processing, 101*, 166–176. https://doi.org/10.1016/j.fbp.2016.11.006

Alpizar-Reyes, E., Román-Guerrero, A., Gallardo-Rivera, R., Varela-Guerrero, V., Cruz-Olivares, J., & Pérez-Alonso, C. (2018). Rheological properties of tamarind (*Tamarindus indica* L.) seed mucilage obtained by spray drying as a novel source of

hydrocolloid. *International Journal of Biological Macromolecules, 107*(part A), 817–824. https://doi.org/10.1016/j.ijbiomac.2017.09.048
Alpizar-Reyes, E., Varela-Guerrero, V., Cruz-Olivares, J., Carrillo-Navas, H., Alvarez-Ramirez, J., & Pérez-Alonso, C. (2020). Microencapsulation of sesame seed oil by tamarind seed mucilage. *International Journal of Biological Macromolecules, 145*, 207–215. https://doi.org/10.1016/j.ijbiomac.2019.12.162
Bajac, J., Nikolovski, B., Loncarevic, I., Petrovic, J., Bajac, B., Durovic, S., & Petrovic, L. (2022). Microencapsulation of juniper berry essential oil (*Juniperus communis* L.) by spray drying: microcapsule characterization and release kinetics of the oil. *Food Hydrocolloids, 125*, Article 107430. https://doi.org/10.1016/j.foodhyd.2021.107430
Bakry, A. M., Fang, Z., Ni, Y., Cheng, H., Chen, Y. Q., & Liang, l (2016). Stability of tuna oil and tuna oil/peppermint oil blend microencapsulated using whey protein isolate in combination with carboxymethyl cellulose or pullulan. *Food Hydrocolloids, 60*, 559–571. https://doi.org/10.1016/j.foodhyd.2016.04.026
Ban, M. T., Mahadin, N., & Abd Karim, K. J. (2022). Synthesis of hydrogel from sugarcane bagasse extracted cellulose for swelling properties study. *Materials Today: Proceedings, 50*, 2567–2575. https://doi.org/10.1016/j.matpr.2021.08.342
Bannikova, A., Evteev, A., Pankin, K., Evdokimov, I., & Kasapis, S. (2018). Microencapsulation of fish oil with alginate: In-vitro evaluation and controlled release. *LWT - Food Science and Technology, 90*, 310–315. https://doi.org/10.1016/j.lwt.2017.12.045
Beirão da Costa, S., Duarte, C., Bourbon, A. I., Pinheiro, A. C., Januário, M. I. N., Vicente, A. A., Beirão da Costa, M. L, & Delgadillo, I. (2013). Inulin potential for encapsulation and controlled delivery of *Oregano* essential oil. *Food Hydrocolloids, 33*, 199–206. https://doi.org/10.1016/j.foodhyd.2013.03.009
Beirão da Costa, S., Duarte, C., Bourbon, A. I., Pinheiro, A. C., Serra, A. T., Martins, M. M., Januário, M. I. N., Vicente, A. A., Delgadillo, I., Duarte, C., & Beirão da Costa, M. L. (2012). Effect of the matrix system in the delivery and in vitro bioactivity of microencapsulated Oregano essential oil. *Journal of Food Engineering, 110*, 190–199. https://doi.org/10.1016/j.jfoodeng.2011.05.043
Benavides, S., Cortés, P., Parada, J., & Franco, W. (2016). Development of alginate microspheres containing thyme essential oil using ionic gelation. *Food Chemistry, 204*, 77–83. https://doi.org/10.1016/j.foodchem.2016.02.104
Bera, H., Boddupalli, S., Nandikonda, S., Kumar, S., & Nayak, A. K. (2015). Alginate gel-coated oil-entrapped alginate–tamarind gum–magnesium stearate buoyant beads of risperidone. *International Journal of Biological Macromolecules, 78*, 102–111. https://doi.org/10.1016/j.ijbiomac.2015.04.001
Boostani, S., & Jafari, S. M. (2021). A comprehensive review on the controlled release of encapsulated food ingredients; fundamental concepts to design and applications. *Trends in Food Science & Technology, 109*, 303–321. https://doi.org/10.1016/j.tifs.2021.01.040
Bušić, A., Belščak-Cvitanović, A., Cebin, A. V., Karlović, S., Kovač, V., Špoljarić, I., Mršić, G., & Komes, D. (2018). Structuring new alginate network aimed for delivery of dandelion (Taraxacum officinale L.) polyphenols using ionic gelation and new filler materials. *Food Research International, 111*, 244–255. https://doi.org/10.1016/j.foodres.2018.05.034
Carneiro, H. C. F., Tonon, R. V., Grosso, C. R. F., & Hubinger, M. D. (2013). Encapsulation efficiency and oxidative stability of flaxseed oil microencapsulated by spray drying using different combinations of wall materials. *Journal of Food Engineering, 115*(4), 443–451. https://doi.org/10.1016/j.jfoodeng.2012.03.033
Chan, E. S. (2011). Preparation of Ca-alginate beads containing high oil content: Influence of process variables on encapsulation efficiency and bead properties. *Carbohydrate Polymers, 84*(4), 1267–1275. https://doi.org/10.1016/j.carbpol.2011.01.015
Chen, F., Deng, Z., Zhang, Z., Zhang, R., Xu, Q., Fan, G., Luo, T., & McClements, D. J. (2018). Controlling lipid digestion profiles using mixtures of different types of microgel: Alginate beads and carrageenan beads. *Journal of Food Engineering, 238*, 156–163. https://doi.org/10.1016/j.jfoodeng.2018.06.009
Chew, S. C., Tan, C. P., & Nyam, K. L. (2018). Microencapsulation of refined kenaf (*Hibiscus cannabinus* L.) seed oil by spray drying using β-cyclodextrin/gum arabic/sodium caseinate. *Journal of Food Engineering, 237*, 78–85. https://doi.org/10.1016/j.jfoodeng.2018.05.016
Corstens, M. N., Berton-Carabin, C. C., Elichiry-Ortiz, P. T., Hol, K., Troost, F. J., Masclee, A. A. M., & Schroën, K. (2017). Emulsion-alginate beads designed to control in vitro intestinal lipolysis: Towards appetite control. *Journal of Functional Foods, 34*, 319–328. https://doi.org/10.1016/j.jff.2017.05.003
da Silva Soares, B., Siquiera, R. P., de Carvalho, M. G., Vicente, J., & Garcia-Rojas, E. E. (2019). Microencapsulation of sacha inchi oil (*Plukenetia volubilis* L.) using complex coacervation: Formation and structural characterization. *Food Chemistry, 298*, Article e125045. https://doi.org/10.1016/j.foodchem.2019.125045
Dangi, D., Mattoo, M., Kumar, V., & Sharma, P. (2022). Synthesis and characterization of galactomannan polymer hydrogel and sustained drug delivery. *Carbohydrate Polymer Technologies and Applications, 4*, Article 100230. https://doi.org/10.1016/j.carpta.2022.100230
Dash, S., Murthy, P. N., Nath, L., & Chowdhury, P. (2010). Kinetic modeling on drug release from controlled drug delivery systems. *Acta Poloniae Pharmaceutica – Drug Research, 67*(3), 217–223. ISSN 0001-6837.
Dehnad, D., Jafari, S. M., & Afrasiabi, M. (2016). Influence of drying on functional properties of food biopolymers: From traditional to novel dehydration techniques. *Trends in Food Science & Technology, 57*, 116–131. https://doi.org/10.1016/j.tifs.2016.09.002
Di Giorgio, L., Salgado, P. R., & Mauri, A. N. (2019). Encapsulation of fish oil in soybean protein particles by emulsification and spray drying. *Food Hydrocolloids, 87*, 891–901. https://doi.org/10.1016/j.foodhyd.2018.09.024
Dima, C., Pătrașcu, L., Cantaragiu, A., Alexe, P., & Dima, Ș. (2016). The kinetics of the swelling process and the release mechanisms of *Coriandrum sativum* L. essential oil from chitosan/alginate/inulin microcapsules. *Food Chemistry, 195*, 39–48. https://doi.org/10.1016/j.foodchem.2015.05.044
Dyab, A. K. F., Mohamed, M. A., Meligi, N. M., & Mohamed, S. K. (2018). Encapsulation of erythromycin and bacitracin antibiotics into natural sporopollenin microcapsules: antibacterial, cytotoxicity, *in vitro* and *in vivo* release studies for enhanced bioavailability. *RSC Advances, 8*, 33432–33444. https://doi.org/10.1039/c8ra05499a
e Silva, K. F. C., da Silva Carvalho, A. N., Rabelo, R. S., & Hubinger, M. D. (2019). Sacha inchi oil encapsulation: Emulsion and alginate beads characterization. *Food and Bioproducts Processing, 116*, 118–129. https://doi.org/10.1016/j.fbp.2019.05.001
Farhoosh, R. (2021). Critical kinetic parameters and rate constants representing lipid peroxidation as affected by temperature. *Food Chemistry, 340*, Article 128137. https://doi.org/10.1016/j.foodchem.2020.128137
Fernandes, R. V. B., Borges, S. V., & Botrel, D. A. (2013). Influence of spray drying operating conditions on microencapsulated rosemary essential oil properties. *Ciência e Tecnologia de Alimentos, 33*(1), 171–178. ISSN 0101-2061.
Goyal, A., Sharma, V., Sihag, M. K., Arora, S., Singh, A. K., & Sabikhi, L. (2016). Effect of microencapsulation and spray drying on oxidative stability of flaxseed oil and its release behavior under simulated gastrointestinal conditions. *Drying Technology, 34*(6), 810–821. https://doi.org/10.1080/07373937.2015.1081929
Kassem, A. A., Farid, R. M., Issa, D. A. E., Khalil, D. S., Abd-El-Razzak, M. Y., Saudi, H. I., Eltokhey, H. M., & El-Zamarany, E. A. (2015). Development of mucoadhesive microbeads using thiolated sodium alginate for intrapocket delivery of resveratrol. *International Journal of Pharmaceutics, 487*(1-2), 305–313. https://doi.org/10.1016/j.ijpharm.2015.04.010
Langyan, S., Yadava, P., Sharma, S., Gupta, N. C., Bansal, R., Yadav, R., Kalia, S., & Kumar, A. (2022). Food and nutraceutical functions of sesame oil: An underutilized crop for nutritional and health benefits. *Food Chemistry, 389*, Article 132990. https://doi.org/10.1016/j.foodchem.2022.132990
Li, J., Jia, X., & Yin, L. (2021). Hydrogel: Diversity of Structures and Applications in Food Science. *Food Reviews International, 37*(3), 313–372. https://doi.org/10.1080/87559129.2020.1858313
Li, D., Wei, Z., & Xue, C. (2021). Alginate-based delivery systems for food bioactive ingredients: An overview of recent advances and future trends. *Comprehensive Reviews in Food Science and Food Safety, 20*(6), 5345–5369. https://doi.org/10.1111/1541-4337.12840
López Córdoba, A., Deladino, L., & Martino, M. (2013). Effect of starch filler on calcium-alginate hydrogels loaded with yerba mate antioxidants. *Carbohydrate Polymers, 95*, 315–323. https://doi.org/10.1016/j.carbpol.2013.03.019
López-Ortiz, A., Rodríguez-Ramírez, J., & Méndez-Lagunas, L. (2016). True density prediction of garlic slices dehydrated by convection. *Journal of Food Science, 81*(1), E49–E55. https://doi.org/10.1111/1750-3841.13187
Lozano-Vazquez, G., Lobato-Calleros, C., Escalona-Buendia, H., Chavez, G., Alvarez-Ramirez, J., & Vernon-Carter, E. J. (2015). Effect of the weight ratio of alginate-modified tapioca starchon the physicochemical properties and release kinetics of chlorogenic acid containing beads. *Food Hydrocolloids, 48*, 301–311. https://doi.org/10.1016/j.foodhyd.2015.02.032
Luna-Guevara, J. J., Ochoa-Velasco, C. E., Hernández-Carranza, P., & Guerrero-Beltrán, J. A. (2017). Microencapsulation of walnut, peanut and pecan oils by spray drying. *Food Structure, 12*, 26–52. https://doi.org/10.1016/j.foostr.2017.04.001
Maderuelo, C., Zarzuelo, A., & Lanao, J. M. (2011). Critical factors in the release of drugs from sustained release hydrophilic matrices. *Journal of Controlled Release, 154*, 2–19. https://doi.org/10.1016/j.jconrel.2011.04.002
Menin, A., Zanoni, F., Vakarelova, M., Chignola, R., Donà, G., Rizzi, C., Mainente, F., & Zoccatelli, G. (2018). Effects of microencapsulation by ionic gelation on the oxidative stability of flaxseed oil. *Food Chemistry, 219*, 293–299. https://doi.org/10.1016/j.foodchem.2018.06.144
Premi, M., & Sharma, H. K. (2017). Effect of different combinations of maltodextrin, gum arabic and whey protein concentrate on the encapsulation behavior andoxidative stability of spray dried drumstick (*Moringa oleifera*) oil. *International Journal of Biological Macromolecules, 105*, 1232–1240. https://doi.org/10.1016/j.ijbiomac.2017.07.160
Siepmann, J., & Peppas, N. A. (2001). Modeling of drug release from delivery systems based on hydroxypropyl methylcellulose (HPMC). *Advance Drug Delivery Reviews, 48*, 139–157. https://doi.org/10.1016/j.addr.2012.09.028
Smaniotto, F., Zafeiri, I., Prosapio, V., & Spyropoulos, F. (2021). Understanding the encapsulation and release of small molecular weight model actives from alginate fluid gels. *Food Structure, 27*, Article 100179. https://doi.org/10.1016/j.foostr.2021.100179
De, Sudipto K., Aluru, N. R., Johnson, B., Crone, W. C., Beebe, D. J., & Moore, J (2002). Equilibrium swelling and kinetics of pH-responsive hydrogels: Models, experiments, and simulations. *Journal of Microelectromechanical systems, 11*(5), 544–555. https://doi.org/10.1109/JMEMS.2002.803281
Ubeyitogullari, A., Ahmadzadeh, S., Kandhola, G., & Kim, J-W. (2022). Polysaccharide-based porous biopolymers for enhanced bioaccessibility and bioavailability of bioactive food compounds: Challenges, advances, and opportunities. *Comprehensive Reviews in Food Science and Food Safety, 21*(6), 4610–4639. https://doi.org/10.1111/1541-4337.13049
Us-Medina, U., Ruiz-Ruiz, J. C., Quintana-Owen, P., & Segura-Campos, R. (2017). *Salvia hispanica* mucilage-alginate properties and performance as an encapsulation matrix for chia seed oil. *Journal of Food Processing and Preservation, 2017*, e13270. https://doi.org/10.1111/jfpp.13270
Velázquez-Gutiérrez, S. K., Alpizar-Reyes, E., Cruz-Olivares, J., Barrera-Pichardo, J. F., Rodríguez-Huezo, M. E., & Pérez-Alonso, C. (2020). Ionic gelation encapsulation of

sesame oil with sodium alginate-nopal mucilage blends: Encapsulation efficiencyand oxidative stability. *Revista Mexicana de Ingeniería Química, 19*(1), 349–362. https://doi.org/10.24275/rmiq/Alim1655

Velázquez-Gutiérrez, S. K., Alpizar-Reyes, E., Guadarrama-Lezama, A. Y., Báez-González, J. G., Alvarez-Ramirez, J., & Pérez-Alonso, C. (2021). Influence of the wall material on the moisture sorption properties and conditions of stability of sesame oil hydrogel beads by ionic gelation. *LWT-Food Science and Technology, 140*, Article e110695. https://doi.org/10.24275/rmiq/Alim1642

Wu, Z., He, Y., Chen, L., Han, Y., & Li, C. (2014). Characterization of *Raoultella planticola* Rs-2 microcapsule prepared with a blend of alginate and starch and its release behavior. *Carbohydrate Polymers, 110*, 259–267. https://doi.org/10.1016/j.carbpol.2014.04.011

Xu-Yan, D., Ping-Ping, L., Fang, W., Mu-lan, J., Ying-Zhong, Z., Guang-Ming, L., Hong, C., & Yuan-Di, Z. (2012). The impact of processing on the profile of volatile compounds in sesame oil. *European Journal of Lipid Science and Technology, 114*, 277–286. https://doi.org/10.1002/ejlt.201100059

Yamashita, C., Moraes, I. C. F., Ferreira, A. G., Branco, C. C. Z., & Branco, I. G. (2021). Multi-response optimization of alginate bleaching technology extracted from brown seaweeds by an eco-friendly agent. *Carbohydrate Polymers, 251*, Article 116992. https://doi.org/10.1016/j.carbpol.2020.116992

Zeeb, B., Saberi, A. H., Weiss, J., & McClements, D. J. (2015). Retention and release of oil-in-water emulsions from filled hydrogel beads composed of calcium alginate: impact of emulsifier type and pH. *Soft Matter, 11*(11), 2228–2236. https://doi.org/10.1039/C4SM02791D

Zhou, M., Hu, Q., Wang, T., Xue, J., & Luo, Y. (2018). Alginate hydrogel beads as a carrier of low density lipoprotein/pectin nanogels for potential oral delivery applications. *International Journal of Biological Macromolecules, 120*, 859–864. https://doi.org/10.1016/j.ijbiomac.2018.08.135